

# Fibrinogen, Riboflavin, and UVA to Immobilize a Corneal Flap – Molecular Mechanisms

Stacy L. Littlechild,<sup>1,2</sup> Yuntao Zhang,<sup>1</sup> John M. Tomich,<sup>3</sup> and Gary W. Conrad<sup>1,2</sup>

**PURPOSE.** Tissue glue containing fibrinogen (FIB) and riboflavin (RF), upon exposure to long wavelength ultraviolet light (UVA, 365 nm) has been proposed potentially to solve long-standing problems presented by corneal wound and epithelial ingrowth side-effects from laser-assisted in situ keratomileus (LASIK). Data presented in a previous study demonstrated an ability of FIB + RF + UVA to adhere two stromal surfaces; however, to our knowledge no molecular mechanisms have been proposed to account for interactions occurring between corneal extracellular matrix (ECM) and tissue glue molecules. Here, we document several covalent and noncovalent interactions between these classes of macromolecules.

**METHODS.** SDS-PAGE and Western blot techniques were used to identify covalent interactions between tissue glue molecules and corneal ECM molecules in either the presence or absence of RF and UVA, in vitro and ex vivo. Surface plasmon resonance (SPR) was used to characterize noncovalent interactions, and obtain  $k_a$ ,  $k_d$ , and  $K_D$  binding affinity values.

**RESULTS.** SDS-PAGE and Western blot analyses indicated that covalent interactions occurred between neighboring FIB molecules, as well as between FIB and collagen type I (Coll-I) proteins (in vitro and ex vivo). These interactions occurred only in the presence of RF and UVA. SPR data demonstrated the ability of FIB to bind noncovalently to corneal stroma molecules, Coll-I, decorin, dermatan sulfate, and corneal basement membrane molecules, laminin and heparan sulfate – only in the presence of  $Zn^{2+}$ .

**CONCLUSIONS.** Covalent and (zinc-mediated) noncovalent mechanisms involving FIB and stromal ECM molecules contribute to the adhesion created by FIB + RF + UVA. (*Invest Ophthalmol Vis Sci.* 2012;53:5991–6003) DOI:10.1167/iovs.12-10201

The simultaneous presence of fibrinogen (FIB), riboflavin (RF), and long wavelength ultraviolet light (UVA, 365 nm)

has been shown to aid in the immobilization of a corneal flap modeled after that which results from laser assisted in situ keratomileus (LASIK) eye surgery.<sup>1</sup> Based on data from the previous publication, covalent and noncovalent interactions appeared to contribute to adhesion between the studied extracellular matrices, such as the corneal epithelial basement membrane (Epi-BM), stroma, and Descemet's membrane (DM). Our study aims to identify some of the specific interactions that are responsible for the adhesion observed in the former publication.

In previous studies, the application of only RF + UVA (no FIB) has been shown to stop the progression of keratoconus, a disease responsible for gradual corneal thinning, by increasing the stiffness of the corneal tissue.<sup>2</sup> This increased rigidity, induced by RF + UVA, occurs because covalent intra- and inter-molecular crosslinks are created between corneal collagen fibrils,<sup>3,4</sup> and collagen and proteoglycan core proteins, respectively.<sup>5</sup> The RF + UVA treatment protocol includes saturating the corneal stroma with an RF-containing solution and subsequently irradiating the tissue with UVA to activate RF to catalyze crosslink formation through a combination of Type I and Type II mechanisms.<sup>6,7</sup> In short, the Type I mechanism proceeds by exciting the RF molecule to its triplet state; then, the newly created RF triplet directly interacts with its substrate to form substrate free radicals, which continue to react with substrate available within the tissue. The Type II mechanism also begins with the creation of triplet RF, but instead of reacting immediately with a substrate, it reacts with molecular oxygen to produce singlet oxygen.<sup>8,9</sup> Similar to the RF + UVA treatment, use of a fibrinogen glue, FIB + RF + UVA, also uses RF as a photosensitizer and UVA light as an activator, which, as has been demonstrated previously, produces covalent bonds by way of both Type I and Type II mechanisms, suggesting that a reactive oxygen species-dependent mechanism is responsible for the increased adhesion observed in ocular tissues.<sup>6</sup>

The observation made during our earlier study of tissue strip adhesion indicated that the degree of adhesion from FIB + RF + UVA treatment increased as more stromal extracellular matrix (ECM) was exposed to the FIB + RF + UVA, suggesting that either the FIB + RF + UVA treatment had a stronger effect on the molecules that compose the ECM of the stroma than on the molecules of the Epi-BM and DM, and/or that there simply are more molecules in the corneal stroma that interact with FIB compared to basement membranes (BMs).

In exploring the possible mechanisms by which FIB + RF + UVA treatment creates adhesion, one first must determine which molecules in the target tissue (the cornea) are present and available for potential interactions with the main component of the tissue glue, FIB. Abundant molecules in corneal basement membranes include such proteins as laminin (LN), collagen type IV (Coll-IV), and the glycosaminoglycan (GAG) chain, heparan sulfate (HS), and its core protein.<sup>10–15</sup> Next, the corneal stromal ECM is comprised predominately of collagen type I (Coll-I)<sup>16–18</sup> and macromolecules, termed proteoglycans (PGs) that consist of a protein

From the <sup>1</sup>Division of Biology, <sup>3</sup>Department of Biochemistry, Kansas State University, Manhattan, Kansas; and the <sup>2</sup>Mount Desert Island Biological Laboratory, Salisbury Cove, Maine.

Supported by an Undergraduate Outreach Fellowship from the NIH/NCRR Maine IDEA Network of Biomedical Research Excellence (ME-INBRE: 2-P20-RR016463); Johnson Center for Basic Cancer Research, Kansas State University; K-INBRE Award Number P20-RR016475 from the National Center for Research Resources; National Institutes of Health-National Eye Institute (NIH-NEI) Grant NIH EY0000952 (GWC). The authors alone are responsible for the content and writing of the paper.

Submitted for publication May 15, 2012; revised July 19, 2012; accepted July 30, 2012.

Disclosure: S. L. Littlechild, None; Y. Zhang, None; J.M. Tomich, None; G.W. Conrad, None

Corresponding author: Stacy L. Littlechild, Division of Biology – Ackert Hall, Kansas State University, Manhattan, KS 66506-4901; stacy.little08@gmail.com.

core (keratocan [Ker], lumican [Lum], mimecan [Mim], or decorin [Dec]) covalently linked to highly sulfated, thus, negatively charged, GAG chains (keratan sulfate, dermatan sulfate, or chondroitin sulfate-A).<sup>19–21</sup> Specifically, Ker, Lum, and Mim are core proteins linked to keratan sulfate (KS) GAG chains, whereas decorin is bonded covalently to dermatan sulfate (DS) and chondroitin sulfate-A (CSA) GAGs.<sup>20,21</sup>

Next, consideration of possible mechanisms should attempt to address which interactions arise from covalent bonds and which from interactions that are noncovalent. To this end, SDS-PAGE and Western blot analyses were performed on the two most abundant proteins of interest, Coll-I (in the cornea) and FIB (in the glue), in the presence and absence of RF and UVA. These techniques were conducted on isolated FIB and Coll-I molecules *in vitro*, and on corneas *ex vivo*, from which macromolecules subsequently were extracted. Next, surface plasmon resonance (SPR) was used to characterize non-covalent interactions between FIB and corneal proteins/GAGs.

Despite FIB + RF + UVA treatment showing promise to act as a tissue adhesive, to our knowledge no molecular studies have determined the specific interactions that generate adhesion during corneal tissue treatment. Our study tests molecules identified above, native to the cornea, for their abilities to form covalent and/or noncovalent bonds with FIB in an effort to understand the molecular mechanisms for previously observed patterns of strong corneal tissue adhesion.

## MATERIALS AND METHODS

### Materials

Frozen whole rabbit corneas were purchased commercially through Pel-Freez Biologicals (Rogers, AR). Coll-I from bovine skin was purchased from INAMED (Fremont, CA). Protease Inhibitor Cocktail, Coll-IV from human placenta, calcium chloride dihydrate, N-ethyl-N'-(3-dimethylaminopropyl)carbodiimide (EDC), biotin-X-hydrazide, heparin (HEP) sodium salt from bovine intestinal mucosa, FIB from bovine plasma, and riboflavin 5'-monophosphate sodium salt (RF), CSA from bovine trachea, HS proteoglycan, and chondroitin sulfate B (dermatan sulfate, DS) from porcine intestinal mucosa were purchased from Sigma-Aldrich (St. Louis, MO). KS from bovine cornea was purchased from Seikagaku America (East Falmouth, MA), and was purified further by chromatography and chondroitinase ABC (Na salt) treatment. The average molecular weight of KS was approximately 15 kilodalton (kDa). CSA was purified by chemical treatment. Recombinant human lumican protein was purchased from Abnova Corporation (Taipei, Taiwan). Recombinant human decorin and recombinant mouse laminin proteins were purchased from R&D Systems (Minneapolis, MN). Goat anti-bovine fibrinogen IgG was purchased from American Diagnostica, Inc. (Stamford, CT), and rabbit polyclonal antibody to collagen type I (ab34710) was purchased from Abcam Inc. (Cambridge, MA). NuPAGE Novex Tris-Acetate 3 to 8% precast gels (8 cm × 8 cm × 1.5 mm), and chromogenic Western blot kits were purchased from Invitrogen Corporation (Carlsbad, CA). The EZ-Link Sulfo-NHS-LC-Biotinylation Kit was purchased from Pierce (Rockford, IL). Amicon Ultra centrifugal filter (regenerated cellulose 3000 MWCO) was purchased from Millipore (Billerica, MA).

SPR analysis was conducted on a Biacore 3000 instrument, and the data were analyzed using BIAevaluation software 4.1 supplied by GE Healthcare, Biacore Life Sciences Division (Piscataway, NJ). Carboxymethylated dextran (CM5) coated chips, Strep-avidin (SA) coated chips, Biotin CAPture kits, and HEPES buffer with surfactant P20 (HBS-P; 10 mM HEPES, pH 7.4, 150 mM NaCl, 0.005% [vol/vol] Surfactant P20) running buffer also were purchased from GE Healthcare/Biacore.

### Solution Preparation

Experimental solutions used for rabbit cornea tissue treatment were prepared fresh, and included "FIB only" and "FIB + RF" FIB solutions contained 18% (wt/vol, 180 mg/mL, 530 μM) FIB. RF solutions contained 0.26% (wt/vol, 2.6 mg/mL, 54.4 mM) of RF. De-ionized water was used as the solvent in all experimental solutions, as per the protocol of Khadem et al.<sup>6</sup> All experimental solution tubes were wrapped in aluminum foil following preparation to prevent premature photoactivation of RF. A 20% (wt/vol, 400 nM) dextran in 1× PBS (pH 7.2) solution was applied topically to keep rabbit corneas from drying during experimentation.

### Ex Vivo Cornea Treatment

To study covalent interactions caused by the FIB + RF + UVA treatment in actual corneal tissue, Western blots were performed on samples from rabbit corneas treated and untreated *ex vivo* with RF + UVA. These rabbit corneas were prepared as follows: Before extraction, frozen whole rabbit eye globes were placed in 1× PBS to thaw. Once thawed, 8 mm corneal strips were excised from the centermost region of the eye globe, and all surrounding sclera was discarded. Next, the epithelium was removed from the anterior surface of each strip using a spatula, and the DM was removed from the posterior surface using jeweler's forceps, thus exposing the posterior stromal surface. Next, 30 μL of the experimental solution (FIB only or FIB + RF) was applied evenly on the exposed stromal surface of one strip. Finally, a second rabbit corneal strip was placed directly on top of the bottom strip containing the layer of experimental solution, so that both exposed stromal surfaces were in contact with each other.

The corneal pairs were allowed to incubate in this orientation for 30 minutes and were kept from drying by administering topically a 20% dextran solution at 10 μL/min using a syringe pump. Experimental corneas then were irradiated for an additional 30 minutes with UVA light (365 nm, 3 mW/cm<sup>2</sup> intensity) 50 mm below the light source while the 20% dextran drip continued to prevent drying of the tissue. Control corneas were not exposed to UVA light, but still were allowed an additional 30 minutes of incubation while dextran prevented tissue drying. Once the incubation and irradiation phases of treatment were through, corneal pairs were snap-frozen immediately and processed for tissue extraction (described below).

### Guanidine-HCl Extraction of Corneal Tissue

The corneal pairs (0.7 g wet weight) treated or untreated with RF + UVA were frozen immediately by liquid nitrogen following treatment, pulverized, homogenized further in 4 M guanidine-HCl (GdnHCl) containing protease inhibitors, and then incubated for 24 hours at 0 to 4°C with gentle agitation. The tissue residue was removed by centrifugation at 10,000 × g for 30 minutes, and the supernatant was retained as the extract. The tissue residue pellet was re-extracted for a second 24 hours with fresh 4 M GdnHCl solution. The two extracts were combined together, neutralized by the addition of 1 M NaOH, and then applied to an Amicon Ultra centrifugal filter (regenerated cellulose 3000 molecular weight [MW] cutoff; Millipore), centrifuged to desalt, and concentrated to 1/5 of the original volume. The filter retentates were used for collagen crosslinking evaluation without any further processing.<sup>5</sup>

### Sodium Dodecyl Sulfate Polyacrylamide Gel Electrophoresis

To test for covalent interactions between neighboring FIB molecules and the most abundant protein of the corneal stromal ECM, Coll-I, electrophoretic gels were run using samples prepared in the presence and absence of RF and UVA light. FIB samples were prepared fresh in phosphate buffer (pH 7.2) at a concentration of 18 μg/μL, and freshly prepared Coll-I samples were prepared at a concentration of 6 μg/μL.

RF was added to samples as a 0.1% RF phosphate buffer addition at physiologic pH 7.2. Experimental sample solutions were exposed to 30 minutes of long wavelength UVA light (365 nm, 3 mW/cm<sup>2</sup> intensity) 50 mm below the light source and were vortexed every 10 minutes during irradiation to prevent potentially crosslinked molecules from collecting at the surface of the sample. (Because of the small volume of each sample [~20  $\mu$ L], vortexing samples every 10 minutes was more practical than continuously stirring the solution using a stir bar and stir plate.)

Immediately following irradiation, 5  $\mu$ L of NuPAGE LDS sample buffer and 2  $\mu$ L of NUPAGE reducing agent were added to each sample, vortexed, heated at 70°C for 10 minutes, and then loaded onto NuPAGE Novex Tris-Acetate 3 to 8% gels (8 cm  $\times$  8 m  $\times$  1.5 mm pre-cast gel) and subjected to electrophoresis (100 mA/gel for 60 minutes) under reducing conditions, using NuPAGE sample reducing agent. Following electrophoresis, the gels were retrieved and rinsed 3 times for 5 minutes each with 2 $\times$  glass distilled water, and then a 0.1% (wt/vol) Coomassie Brilliant Blue R-250 solution was used to stain protein in the gel.

Since the strength of the adhesion created by the FIB + RF + UVA treatment increases as interval between UVA-irradiation and mechanical testing increases,<sup>22</sup> it was important to keep this time consistent in mechanical and molecular tests. To achieve this consistency, all samples were prepared to load onto an SDS-PAGE gel immediately following UVA irradiation. No samples were treated by UVA and then stored for any time before performing molecular tests, such as SDS-PAGE and/or WB.

## Western Blots

To increase sensitivity for detecting protein-protein interactions between FIB and Coll-I in vitro and ex vivo, these interactions were characterized further using Western blot analysis. Immediately following gel electrophoresis, proteins were electroblotted (Mini Trans-Blot Electrophoretic Transfer cell; Bio-Rad, Hercules, CA) onto nitrocellulose (Fisher Scientific, Waltham, MA) instead of staining with Coomassie Brilliant Blue R-250. Protein transfer buffer was prepared according to Bio-Rad instructions: pH 8.3, 25 mM Tris, 192 mM glycine and 0.05% (wt/vol) SDS in 20% methanol. The voltage to transfer the proteins was 100 V and was applied for 1 hour. To avoid over-heating the system, the transfer unit was packed in ice for the duration of the transfer. Following transfer, chromogenic immunodetection for small membranes was performed following the kit protocol (Invitrogen). Fibrinogen and Coll-I proteins were identified using anti-fibrinogen antibody and anti-collagen type I antibody, respectively.

## Surface Plasmon Resonance

SPR was used to detect noncovalent FIB—bGAG and FIB—protein interactions. All buffer and sample solutions were de-gassed and vacuum filtered (pore size 0.22  $\mu$ m) before running through the Biacore microfluidic system during immobilization and experimentation procedures. Two types of chips were used to study protein or GAG interactions with FIB. First, CM5 chips were used to immobilize proteins (Fig. 1a); for simplicity, these chips henceforth will be referred to as “protein chips.” To immobilize biotinylated GAGs, SA chips were used (Fig. 1b); these chips will be referred to simply as “GAG chips” hereafter.

The immobilization procedure used to covalently attach proteins on a protein chip has been specifically described elsewhere.<sup>23,24</sup> Briefly, an equal volume mixture of EDC and NHS (0.2 M, 0.05 M, respectively) activated the carboxymethylated surface on each of four total lanes on the chip. Next, a 100  $\mu$ g/mL solution consisting of the ligand (molecule to be immobilized: FIB, Coll-I, Dec, Lum, Coll-IV, or LN) in 10 mM sodium acetate buffer (pH 4.5) was injected at a rate of 5  $\mu$ L/minutes by the autosampler over the activated chip surface for 2 to 6 minutes, depending on the desired level of immobilized ligand. A 1 M ethanolamine hydrochloride solution (pH 8.5) injection followed that of the ligand solution to convert remaining reactive ester groups on the

chip surface to amides.<sup>23</sup> A control lane (lane 1) on each chip was “inactivated” by treating it with HBS-P buffer instead of a ligand solution. Ligand immobilization levels varied from 4000 to 6000 response units (RU), depending on the molecule immobilized, and were controlled by adjusting the amount of time the ligand solution was allowed to react with the activated chip surface. A response of 1000 RU corresponded to 1 ng/mm<sup>2</sup> surface protein concentration.<sup>25</sup>

To immobilize GAGs on the surface of an SA (GAG) chip, it first was necessary to couple covalently biotin molecules to the GAG chain. Once biotinylated (described below), GAGs were exposed to the avidin-coated chip surface during the immobilization procedure. The strong interaction between biotin molecules on the GAG chain and avidin molecules on the chip surface provided a stable bond to immobilize GAGs and prevent their dissociation during experimentation. GAG chip immobilization also has been described previously in detail.<sup>26</sup> Briefly, a GAG chip was conditioned with 1 M NaCl in 50 mM NaOH for three 1-minute pulses. Immediately following, 0.1 mg/mL solutions of biotinylated GAGs (bGAGs; bCSA, bKS, bHS, bDS, or bHEP) were allowed to flow over the surface of the conditioned chip for 3 minutes at a rate of 5  $\mu$ L/minutes. A saturated solution of biotin was immobilized on lane 1 of the GAG chip as a control.<sup>27</sup> Immobilized bGAG levels ranged from 400 to 600 RU, depending on the molecule; the immobilized biotin control reached a level of 30 to 50 RU.

Binding assays were performed using the KINJECT feature of the Biacore 3000; this feature allowed the association rate constant ( $k_a$ ) and the dissociation rate constant ( $k_d$ ) to be studied in real time. Analyte solutions were passed over chip surfaces at a rate of 10  $\mu$ L/min for 5 minutes. Unbound analyte then was allowed to dissociate from the ligand surface for 5 minutes as running buffer (HBS-P) flowed over the chip at a constant rate of 10  $\mu$ L/min. Data from the “inactivated” (protein chip) or biotin-immobilized (GAG chip) control (lane 1) were subtracted out automatically as control background from data collected in experimental lanes containing immobilized ligand (lanes 2–4).

A 1 M NaCl solution was used to regenerate the ligand surface when testing protein-protein interactions on a protein chip. When testing bGAG-protein interactions on a GAG chip, 1 M NaCl in 50 mM NaOH was used for regenerating the chip surface.

## Preparation of Biotinylated KS

KS was biotinylated as described previously in detail.<sup>26</sup> In brief, EDC protocol<sup>28,29</sup> was used to affix biotin to the KS chain. KS was dissolved in MES ([2-N-morpholino] ethanesulfonic acid) containing biotin-LC-hydrazide and EDC. The mixture was agitated gently and incubated 24 hours at room temperature. Biotinylated KS solution was washed thoroughly using a centrifugal filter (regenerated cellulose 3000 MWCO) to remove salt and free biotin; the retentate then was lyophilized. The HABA assay for measuring the level of biotin incorporation was used to calculate the biotinylation ratio, 1.43 moles biotin per mole KS. No biotin molecules were bonded along the length of KS chains, because KS chains do not contain free carboxyl groups.<sup>30</sup> Instead, a biotin molecule was bonded at the reducing-carbon end of each KS chain.

## Preparation of Biotinylated CSA, DS, HS, and HEP

Chains of CSA, DS, HS, and HEP were biotinylated as described previously.<sup>26</sup> Briefly, CSA, DS, HS, and HEP were labeled by EZ-link Biotin-LC-Hydrazide: biotin was attached to the carboxy groups of uronic acid (CSA)<sup>31</sup> or L-iduronic acid (DS, HS, HEP)<sup>32–35</sup> residues using the EDC protocol.<sup>28,29</sup> Unlike the end-labeling of KS chains, CS, DS, and HS chains contained biotin molecules attached along their lengths, not just at their C-reducing end. GAGs were dissolved in MES containing biotin-LC-hydrazide and EDC. The mixture was agitated gently and incubated at room temperature for 24 hours. Biotinylated GAG solutions were washed thoroughly to remove salt and free biotin using an Amicon Ultra centrifugal filter (regenerated cellulose 3000 MWCO), and then were lyophilized. The HABA assay for measuring the

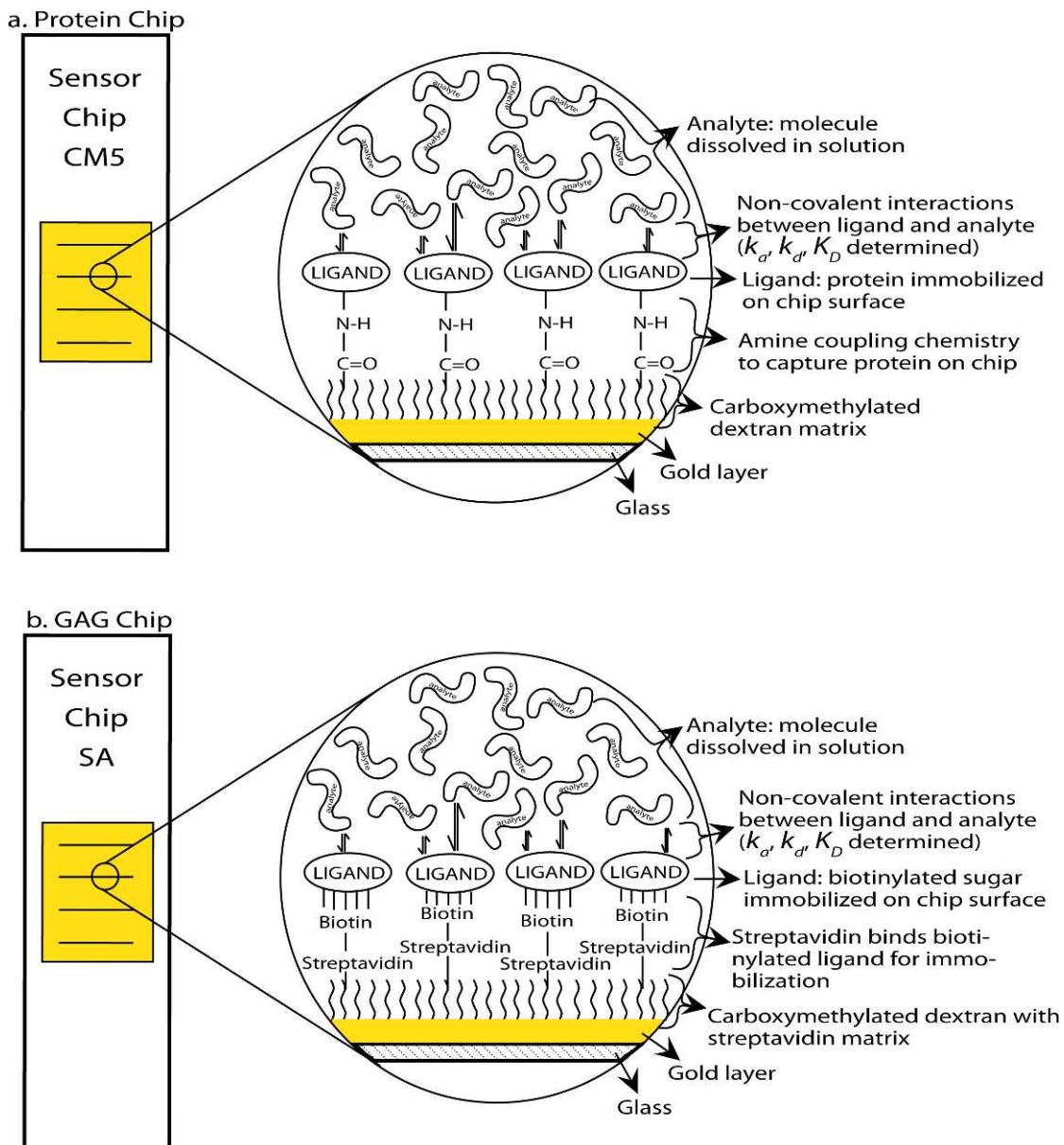


**FIGURE 1.** (a) The surface of the CM5 (protein) chip. Four lanes on each protein chip are connected sequentially (tandem connecting channels not shown). Each lane is composed of a glass foundation with a gold layer on top. The protein chip has a carboxymethylated dextran matrix with free carboxyl groups designed to capture covalently amine groups of the protein to be immobilized. (b) The surface of an SA (GAG) chip (tandem connecting channels not shown). Here, there are glass, gold, and carboxymethylated dextran foundations, as in the chip above, but in addition there is immobilized streptavidin. The streptavidin is designed to link strongly to biotinylated ligands.

level of biotin incorporation was used to determine the molar ratio of biotinylation, 2.78 moles biotin per mole GAG.

### Statistical Analysis

All data presented in tables were analyzed statistically and presented as an average  $\pm$  SD.

## RESULTS

### Sodium Dodecyl Sulfate Polyacrylamide Gel Electrophoresis

Proteins were separated by SDS-PAGE to assay for covalent interactions resulting from treatment with RF + UVA. Figure 2

shows the variety of such binding patterns of FIB (Fig. 2a) and of Coll-I (Fig. 2b). Two lanes of each control were run at different volumes of FIB to determine which volume showed the clearest results on the gel. Lanes 2, 4, 6, and 8 were run at a lower, clearer volume (2  $\mu$ L at 18  $\mu$ g/ $\mu$ L = 32  $\mu$ g FIB), whereas lanes 3, 5, 7, and 9 were run at a higher volume (3  $\mu$ L at 18  $\mu$ g/ $\mu$ L = 54  $\mu$ g FIB). In light of this, 32  $\mu$ g of FIB at a concentration of 18  $\mu$ g/ $\mu$ L was the chosen volume used in subsequent gels. Lanes 2 and 3 in Figure 2a demonstrate the expected locations of untreated fibrinogen subunit bands, alpha, beta, and gamma ( $\alpha$ ,  $\beta$ , and  $\gamma$ , respectively) at 73, 60, and 53 kDa, respectively.<sup>36</sup> FIB molecules, following addition of only RF, are shown in lanes 4 and 5, and FIB molecules, treated only with UVA, are shown in lanes 6 and 7. No crosslinking was observed in lanes 4 to 7; this is evident in that  $\alpha$ ,  $\beta$ , and  $\gamma$  bands of the RF-treated

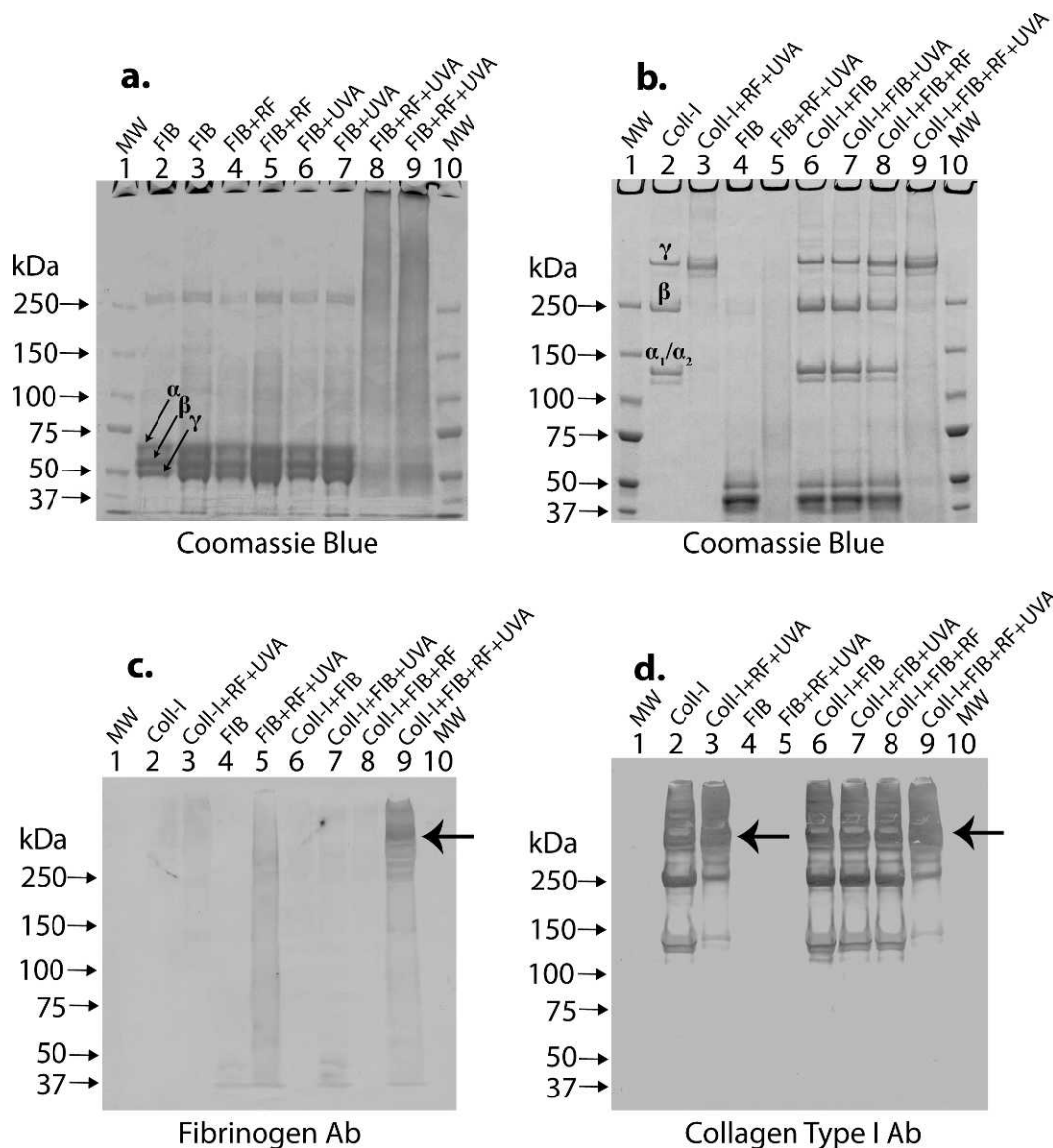


**FIGURE 2.** (a) FIB only covalently crosslinks to itself in the presence of RF and UVA light, as detected by SDS-PAGE. Such crosslinking is observed in lanes 8 and 9, when FIB and RF are present simultaneously with UVA. The  $\alpha$ ,  $\beta$ , and  $\gamma$  chain bands (observed in lanes 2-7) have diminished and generated a spectrum of higher molecular weight molecules, from 100 to 450 kDa. (b) Coll-I and FIB appear to crosslink to each other in the presence of RF and UVA, as detected by SDS-PAGE. Lane 3: Coll-I can crosslink with itself. Lane 5: FIB can crosslink with itself. Maximal crosslinking is observed when Coll-I, FIB, and RF samples are treated with UVA (lane 9). (c) Western blot analysis using FIB antibody shows a difference in crosslinked band patterns in the presence and absence of Coll-I. In the absence of Coll-I, FIB crosslinking creates a spectrum of molecules of increasing molecular size (lane 5). In the presence of Coll-I, a large, dark band appears in the same region of the  $\gamma$ -chain of Coll-I (arrow in lane 9), suggesting Coll-I and FIB crosslink to one another. (d) Western blot analysis of identical samples to those in (c), using Coll-I antibody shows a high molecular weight band (arrows in lanes 3 and 9) when Coll-I + RF (lane 3) or Coll-I + FIB + RF (lane 9) is treated with UVA. That band contains FIB and Coll-I only when both molecules are present simultaneously and treated with RF + UVA.

and the UVA-treated FIB remain at the same molecular weight location as the untreated, standard FIB  $\alpha$ ,  $\beta$ , and  $\gamma$  chain bands. Lastly, FIB incubated with RF and exposed to UVA is shown in lanes 8 and 9 and clearly show diminished  $\alpha$ ,  $\beta$ , and  $\gamma$  chain bands from their usual 73, 60, and 53 kDa location, and show appearance of higher molecular weight FIB in a range from 100 kDa to approximately 450 kDa.

An SDS-PAGE gel also was run with solutions containing FIB and Coll-I present (Fig. 2b). Collagen crosslinked to itself in the presence of RF and UVA (lane 3), and FIB crosslinked to itself in the presence of RF and UVA (lane 5). No crosslinking occurred between Coll-I and FIB in the absence (lane 6) or presence of UVA only (lane 7), or RF only (lane 8). However, lane 9 suggests

that FIB and Coll-I crosslink to each other in the presence of RF and UVA, as the  $\alpha$ ,  $\beta$ , and  $\gamma$  chain bands of FIB virtually disappear, as do the  $\alpha$ -1 (125 kDa),  $\alpha$ -2 (130 kDa), and  $\beta$  (250 kDa) chain bands of Coll-I; Western blots were performed to determine independently whether the two proteins simply crosslinked to themselves and/or each other.

**Western Blots – In Vitro**

The Western blots in Figures 2c and 2d, loaded with identical sets of samples, but probed with different antibodies, show a distinct difference in banding patterns between FIB + RF + UVA lanes and Coll-I + FIB + RF + UVA lanes. Figure 2c (FIB

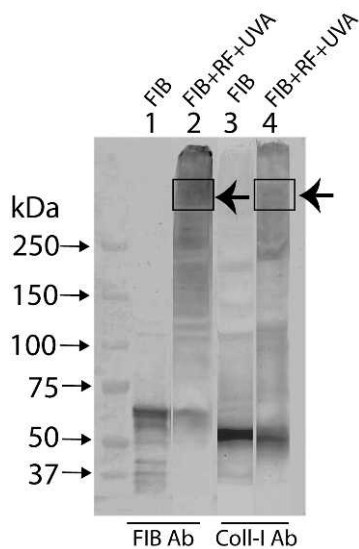


**FIGURE 3.** Western blot analysis of samples extracted from ex vivo rabbit corneas that had been treated with FIB only or with FIB + RF + UVA. Lanes 1 and 2 were developed using a FIB antibody, whereas lanes 3 and 4 were developed using a Coll-I antibody. The low molecular weight bands observed in lane 1 represent standard FIB chains,<sup>36</sup> whereas the low molecular weight band in lane 3 represents the most easily extractable soluble fragment of protease-digested Coll-I (explanation in Discussion). Lanes 2 and 4 are derived from FIB + RF + UVA-treated corneas, and show diminished low molecular weight bands and formation of higher molecular weight bands. Arrows in lanes 2 and 4 indicate a high molecular weight band that corresponds to the  $\gamma$ -chain location of Coll-I.

Ab) shows that the low molecular weight  $\alpha$ ,  $\beta$ , and  $\gamma$  chains of FIB (lane 4) diminish when RF + UVA are introduced and, instead, form a broad range of higher molecular weight molecules ( $\sim 37$  kDa to  $\sim 400$  kDa, lane 5). Furthermore, when Coll-I is introduced to the FIB + RF + UVA mixture, a very dark FIB-staining band is generated in the  $\gamma$ -chain region of Coll-I (arrow in Fig. 2c, lane 9). Similarly, Figure 2d (Coll-I Ab) shows that the  $\alpha_1/\alpha_2$  and  $\beta$  chains of untreated Coll-I (lane 2) diminish in the presence of RF and UVA (lane 3), forming a darker band in the  $\gamma$ -chain region of Coll-I (arrows in lanes 3 and 9).

### Western Blot – Corneas Treated Ex Vivo

Figure 3 shows data collected from rabbit corneas incubated ex vivo with a FIB-only solution (lanes 1 and 3) or with an FIB + RF solution followed by UVA irradiation (lanes 2 and 4). Lanes 1 and 2 were developed using a FIB antibody, whereas lanes 3 and 4 were developed using a Coll-I antibody. The standard low molecular weight location for FIB bands at approximately 73, 60, and 53 kDa<sup>36</sup> are shown in lane 1, whereas lane 2 shows these bands diminished greatly after addition of RF and irradiation with UVA light. Also, lane 2 shows the appearance of a solid high molecular weight band (arrow), similar to that observed in the in vitro data (Fig. 2c, lanes 5, 9). Similar to lanes 1 and 2 (probed with FIB-Ab), lane 3 (probed with Coll-I-Ab) shows a low molecular weight band in the absence of RF + UVA, but upon addition of RF + UVA in lane 4, the intensity of the low molecular weight bands decreases and a strong, high molecular weight band is formed. Finally, a high molecular weight band appears in lanes 2 and 4 that corresponds to the standard location of the Coll-I  $\gamma$ -chain band. These bands are indicated by arrows in Figure 3, lanes 2, 4.

### Surface Plasmon Resonance

Many proteins (FIB, Coll-I, Dec, LN, Coll-IV, Lum) and bGAGs (bCSA, bKS, bDS, bHS and bHep) were tested using SPR for their ability to bind noncovalently FIB in the presence and absence of various divalent cations (1.0 mM  $\text{Ca}^{2+}$ , 2.5 mM  $\text{Ca}^{2+}$ , 1.0 mM  $\text{Zn}^{2+}$ ).<sup>37,38</sup>

Because FIB has been known to denature during SPR experimentation<sup>39</sup> and calcium has been shown to stabilize FIB,<sup>40,41</sup>  $\text{Ca}^{2+}$  was added to analyte (soluble FIB) and running buffer (HBS-P) solutions at two different concentrations, 1.0 mM<sup>40</sup> and 2.5 mM,<sup>42,43</sup> to prevent FIB denaturation. Additionally, in prior studies that characterized binding between FIB and HEP, no binding was detected between FIB and HEP when  $\text{Ca}^{2+}$  was not added to experimental solutions.<sup>39</sup> Conversely, in studies where  $\text{Ca}^{2+}$  was used in experimental solutions, binding was detected between FIB and HEP<sup>44–46</sup> Therefore, the interactions of FIB and bHEP in the presence and absence of  $\text{Ca}^{2+}$  were used as positive controls for this study (indicated by asterisks, Table 1).

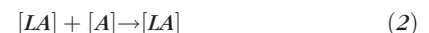
Additionally,  $\text{Zn}^{2+}$  has been shown to mediate highly relevant FIB—protein interactions, specifically the binding of Dec and FIB, in several studies.<sup>47–49</sup> In light of this, Dec—FIB binding in the presence of 1.0 mM  $\text{Zn}^{2+}$  was used as another positive control (indicated by asterisks, Table 1).

Table 1 summarizes binding results of immobilized bGAGs and proteins to soluble FIB. The columns from left to right indicate which, if any, divalent cation (No added cation, “nil”; 1.0 mM  $\text{Ca}^{2+}$ ; 2.5 mM  $\text{Ca}^{2+}$ ; or 1.0 mM  $\text{Zn}^{2+}$ ) was added to the analyte (soluble FIB) and running buffer (HBS-P) solutions. A (–) sign indicates that the two molecules in the intersecting row and column produced a response of less than 20 RU, meaning no significant binding occurred.<sup>50</sup> A (+) sign indicates the molecules in that intersecting row and column produced more than a 20 RU response, meaning those molecules did show binding. None of the studied molecules showed binding to FIB in solutions without a divalent cation. Of the molecules tested, only bHEP could bind FIB in the presence of  $\text{Ca}^{2+}$ . However, when  $\text{Zn}^{2+}$  was present in FIB analyte solutions, bDS and bHS demonstrated the ability to bind, whereas bKS and bCSA did not. Similarly, FIB, Coll-I, Dec, and LN only showed binding to FIB when  $\text{Zn}^{2+}$  was present; Lum and Coll-IV showed no binding, regardless of the divalent cation present (Table 1).

For all molecules that showed binding to soluble FIB, association constants ( $k_a$ ), dissociation constants ( $k_d$ ), and equilibrium dissociation constants ( $K_D$ ) were calculated and compiled into Tables 2 to 4, respectively. All values were calculated assuming that one molecule of ligand (immobilized protein or bGAG) bound one molecule of analyte (FIB in solution), as illustrated by equation (1), where [L] refers to one ligand molecule, [A] refers to one analyte molecule, and [LA] refers to one ligand-analyte complex.



The association constant describes the speed with which the analyte (FIB in solution) binds to the immobilized ligand (bound protein or bGAG) (Fig. 4, dashed curve) and forms ligand-analyte complexes; equation (2) illustrates this interaction.



The faster the analyte binds the ligand, the higher the  $k_a$  value. Dec, LN, and bDS bound FIB the fastest and, thus, have the highest association constants.

Equation (3) below shows the reaction for ligand-analyte complex dissociation; dissociation constants,  $k_d$ , describe the

**TABLE 1.** Binding of Soluble FIB to Immobilized Corneal Macromolecules

Ligand (Molecule on Chip)	Analyte (Molecule in Solution)			
	No Cation	[Ca <sup>2+</sup> ]		[Zn <sup>2+</sup> ]
		Nil	1.0 mM	2.5 mM
	FIB	FIB	FIB	FIB
<b>Proteins</b>				
(on protein chip)				
FIB	-	-	-	+
Coll-I	-	-	-	+
LN	-	-	-	+
Dec	-	-	-	+*
Coll-IV	-	-	-	-
Lum	-	-	-	-
<b>bGAGs</b>				
(on GAG chip)				
bHEP	-*	+*	+	+
bHS	-	-	-	+
bDS	-	-	-	+
bCSA	-	-	-	-
bKS	-	-	-	-

-, indicates no binding detected between two molecules (less than 20 RU response); +, indicates binding detected between two molecules (more than 20 RU response). All molecular combinations that showed binding are described further using graphs to show the effect of calcium and zinc on degree of binding;  $k_a$ ,  $k_d$ , and  $K_D$  values were obtained for all molecular combinations that displayed binding.

\* Indicates positive controls, based on an earlier publication.<sup>50</sup>

speed at which these complexes dissociate (Fig. 4, dotted curve).

$$[L] + [A] \leftarrow [LA] \tag{3}$$

The higher the value of  $k_d$ , the faster the ligand-analyte complexes dissociate into their constituent molecules. The molecules that showed the highest dissociation  $k_d$  values, as shown in Table 3, were FIB, Dec, and LN, only in the presence of 1.0 mM Zn<sup>2+</sup>. Also, bHEP exhibited fast dissociation from immobilized FIB in the presence of 1.0 and 2.5 mM Ca<sup>2+</sup> (Table 3).

The relationship of  $k_a$  and  $k_d$  describes the overall avidity of binding observed between the ligand and the analyte and provides the equilibrium dissociation constant ( $K_D$ ). Equation (4) below is used to determine the  $K_D$  by relating the

**TABLE 2.** Binding of Soluble FIB to Immobilized Corneal Macromolecules: Association Constants (avg.  $k_a \times 10^3 \pm SD \times 10^3$ ) (1/Ms)

	No Cation	[Ca <sup>2+</sup> ]		[Zn <sup>2+</sup> ]
		1.0 mM	2.5 mM	1.0 mM
				Nil
<b>Proteins</b>				
FIB	-	-	-	7.39 ± 0.3
Coll-I	-	-	-	33.9 ± 8.4
Dec	-	-	-	94.9 ± 1.7
LN	-	-	-	84.7 ± 7.2
<b>GAGs</b>				
bDS	-	-	-	79.5 ± 23.5
bHS	-	-	-	5.9 ± 8.6
bHEP	-	10.3 ± 3.2	13.8 ± 1.7	0.59 ± 0.1

**TABLE 3.** Binding of Soluble FIB to Immobilized Corneal Macromolecules: Dissociation Constants ( $k_d \times 10^{-4} \pm SD \times 10^{-4}$ ) (1/s)

	No Cation	[Ca <sup>2+</sup> ]		[Zn <sup>2+</sup> ]	
		Nil	1.0 mM	2.5 mM	1.0 mM
<b>Proteins</b>					
FIB	-	-	-	5.98 ± 0	
Coll-I	-	-	-	0.581 ± 0.1	
Dec	-	-	-	6.63 ± 0.8	
LN	-	-	-	3.22 ± 0.3	
<b>GAGs</b>					
bDS	-	-	-	1.91 ± 0.7	
bHS	-	-	-	0.17 ± 0.01	
bHEP	-	5.52 ± 1.4	6.48 ± 0.47	0.03 ± 0.01	

association and dissociation constants.

$$k_d/k_a = K_D \tag{4}$$

Strong binding between ligands and analytes is characterized by two things, fast association (high  $k_a$ ) and slow dissociation (low  $k_d$ ). Since  $k_a$  is in the denominator and  $k_d$  is in the numerator of equation (4), avid binding is distinguished by low  $K_D$  values. As the association constant increases and the dissociation constant decreases, the overall equilibrium constant decreases. Table 4 summarizes the equilibrium dissociation constants collected. The most avid binding of soluble FIB occurred with immobilized Coll-I, bDS, and bHS, and only in the presence of 1.0 mM Zn<sup>2+</sup>, as these molecular combinations have the lowest  $K_D$  values. The bHEP—FIB  $K_D$  was relatively high in the presence of Ca<sup>2+</sup>, but very low when Zn<sup>2+</sup> was present, indicating avid binding when Zn<sup>2+</sup> was present (Table 4).

To determine whether observed binding between immobilized molecules and soluble FIB was linear or logarithmic, four different concentrations of analyte (soluble FIB) solutions were tested in triplicate and plotted against their resulting response levels (Fig. 4, point a) in Figures 5 to 7. The bold horizontal dashed line in Figures 5 to 7 indicates a 20 RU response, the lowest response above which is considered a significant, positive binding result.<sup>50</sup> The graphed response level was the response collected at the end of the binding curve—after the analyte (soluble FIB) associated and dissociated, but before regeneration of the chip surface (Fig. 4, point a).

Figure 5 shows results for all proteins that demonstrated significant ability to bind soluble FIB in the presence of 1.0 mM

**TABLE 4.** Binding of Soluble FIB to Immobilized Corneal Macromolecules: Equilibrium Dissociation Constants ( $K_D \times 10^{-9} \pm SD \times 10^{-9}$ ) (M)

	No Cation	[Ca <sup>2+</sup> ]		[Zn <sup>2+</sup> ]
		1.0 mM	2.5 mM	1.0 mM
				Nil
<b>Proteins</b>				
FIB	-	-	-	80.8 ± 3.5
Coll-I	-	-	-	1.73 ± 0.1
Dec	-	-	-	6.98 ± 0.7
LN	-	-	-	3.79 ± 0.1
<b>GAGs</b>				
bDS	-	-	-	2.37 ± 0.2
bHS	-	-	-	2.71 ± 0.4
bHEP	-	54.3 ± 5.2	47.1 ± 2.1	4.43 ± 0.8

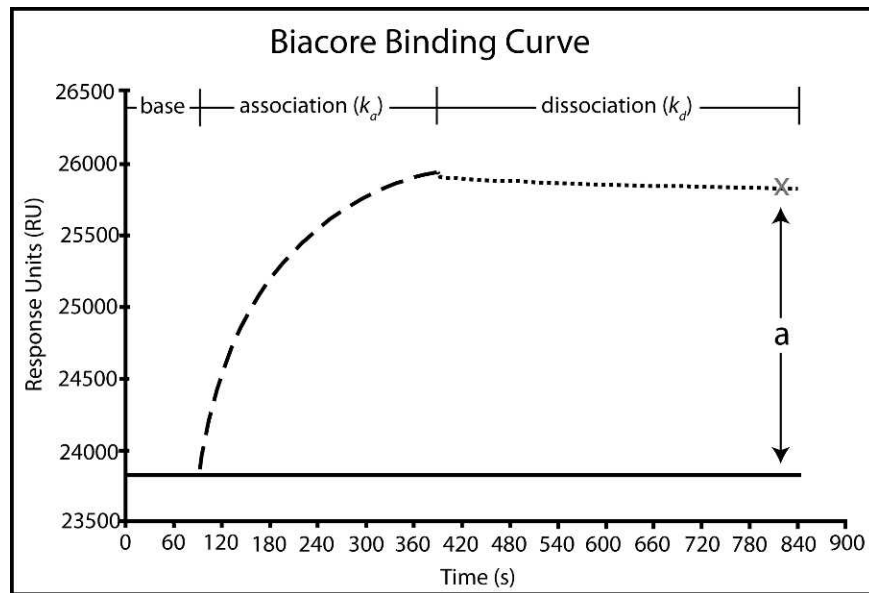


FIGURE 4. The shape of a typical binding curve collected from the Biacore 3000 is shown. The *solid line* at 23,800 RU is the baseline response. *Dashed curve*: indicates the association phase of the curve when the analyte molecule (in solution) is allowed to bind to an immobilized ligand on the chip surface. The association binding constant,  $k_a$ , describes how fast this binding occurs. *Dotted line*: indicates the dissociation phase of the curve, when buffer solution is injected over the chip surface and free analyte molecules (any analyte that is not bound to the ligand surface) are carried away; the rate at which dissociation occurs is described by  $k_d$ , the dissociation constant. Point (a) at the end of the dissociation phase indicates a "report point" where an exact measurement of the response is recorded, relative to the baseline; this value is obtained by subtracting the baseline response from the absolute response (x).

Zn<sup>2+</sup>. Coll-I produced the highest response at all concentrations, followed by immobilized FIB, LN, and Dec. All proteins that bound soluble FIB did so in a linear fashion, as all the lines in Figure 5 are a linear best-fit line of the data points.

Similarly, bHS, bDS, and bHEP linearly bound soluble FIB, as depicted in Figures 6 and 7. Figure 6a shows the binding of bHEP, bDS, and bHS in the presence of 1.0 mM Zn<sup>2+</sup>. The

bHEP—FIB interaction produced the highest response and steepest slope of any of the molecules tested. Because the response of bHEP was so large and dwarfed the still significant results of bDS and bHS, Figure 6b shows bDS and bHS data in the absence of the bHEP line. This simply allows for a clearer presentation of the difference in responses of bDS and bHS. Data in Figure 6, therefore, indicate significant binding of FIB

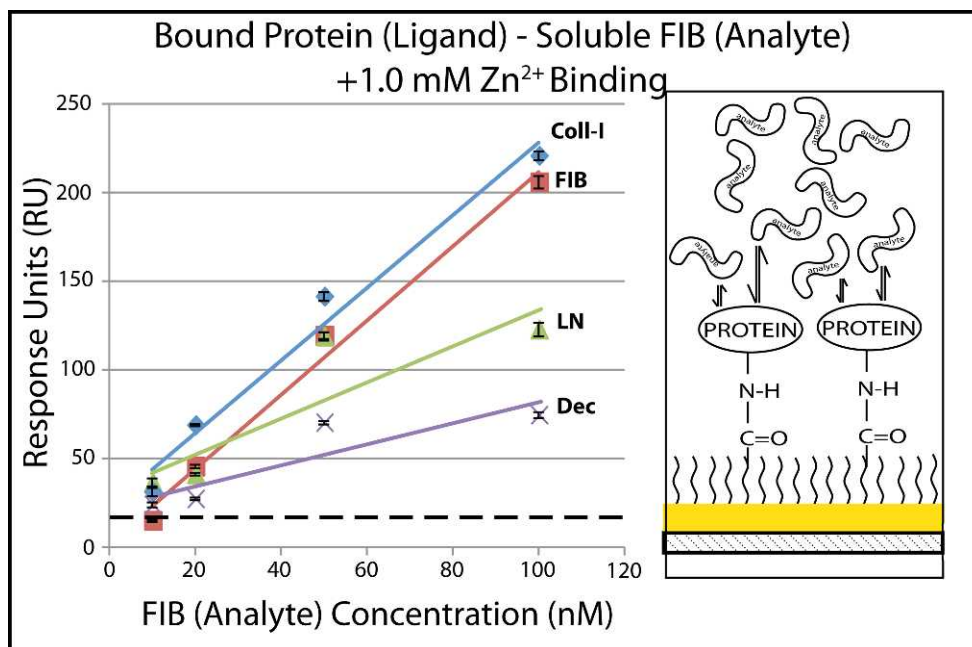
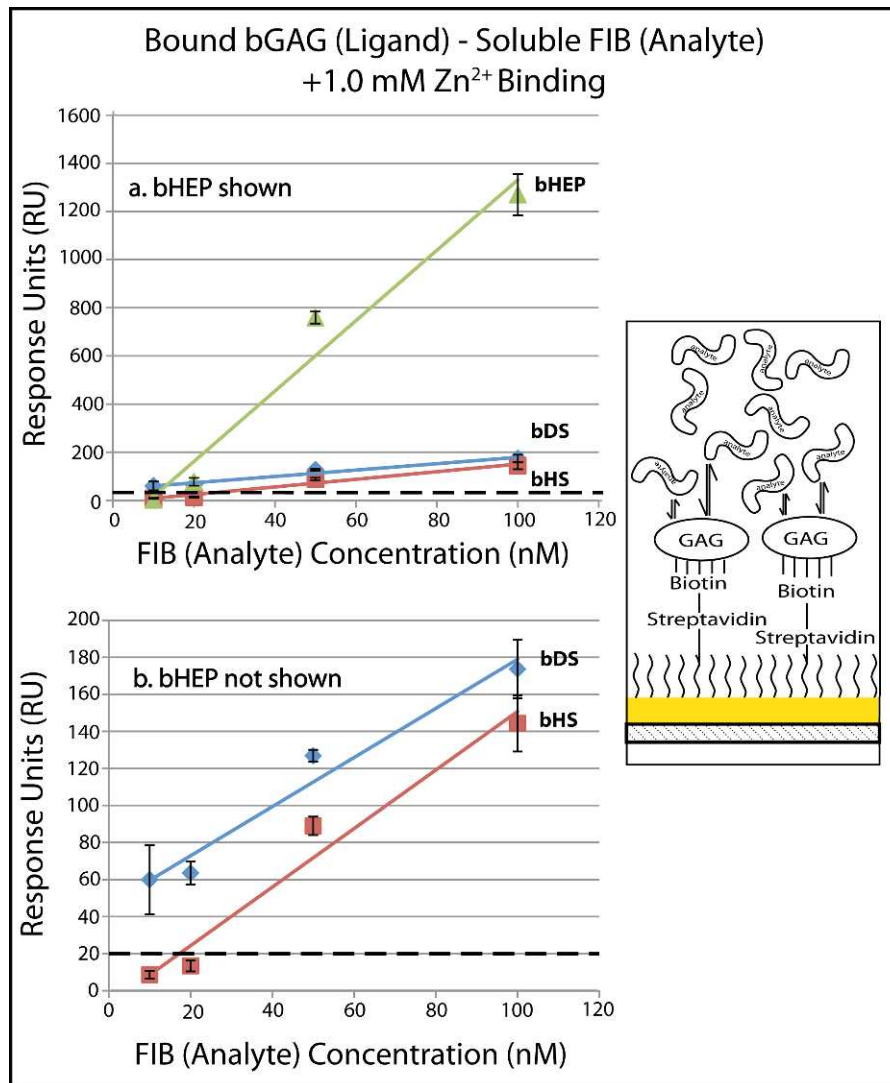


FIGURE 5. The relationship between analyte (soluble FIB + 1.0 mM Zn<sup>2+</sup>) concentration and response at report point (a) of various immobilized proteins. *Bold horizontal dashed line*: indicates the minimum response to be considered a positive binding result. The response of all proteins increased with increasing analyte concentration, and exhibited a linear relationship between analyte concentration and response.



**FIGURE 6.** (a) The relationship between the response at report point (a) of immobilized bGAG and analyte (FIB + 1.0 mM Zn<sup>2+</sup>) are graphed. *Bold horizontal dashed line:* shows the minimum response required to be considered positive binding. All bGAGs show increasing response as analyte concentration increased and a linear relationship. (b) The response of bHEP was so large in (a), it dwarfed the results of bDS and bHS. Here, the response of bHEP is removed to shift the scale of the y-axis, enlarge the results of bDS and bHS, and thus depict more clearly the difference in responses of bDS and bHS.

to DS, a normal component of the corneal stroma, in the presence of Zn<sup>2+</sup>.

Lastly, the binding of immobilized bHEP to soluble FIB in the presence of 0, 1.0, and 2.5 mM Ca<sup>2+</sup> is graphed in Figure 7. As illustrated by the bold horizontal dashed line, no binding occurred between bHEP and soluble FIB in the absence of added Ca<sup>2+</sup>, whereas significant binding did occur at 1.0 and 2.5 mM Ca<sup>2+</sup> concentrations. Interestingly, the FIB+1.0 mM Ca<sup>2+</sup> samples produced a higher response than did the FIB+2.5 mM Ca<sup>2+</sup> samples, suggesting an optimal Ca<sup>2+</sup> concentration.

**DISCUSSION**

The FIB + RF + UVA treatment has been tested for a variety of uses, such as closing corneal<sup>51</sup> and scleral<sup>6,52</sup> incisions following ophthalmic surgery or trauma, replacing sutures in ocular surgeries,<sup>22</sup> and sealing a corneal flap modeling that which results from LASIK.<sup>1</sup> Additionally, extensive research shows FIB + RF + UVA to be a nontoxic, biodegradable glue

that actually can increase rates of wound healing in the cornea.<sup>53,54</sup> However, more work must be done to assess the longevity of FIB + RF + UVA benefits using organ culture techniques, as described by Mi et al.<sup>55</sup> Despite the numerous uses and benefits of the tissue glue, very few studies have attempted to determine the molecular mechanisms that underlie the adhesive properties of FIB + RF + UVA. A deeper understanding of the molecular interactions responsible for the adhesion created in corneas by the FIB + RF + UVA treatment would aid in the further development of the tissue glue and could reveal alternative uses.

By identifying the molecules that interact with FIB in the presence (or absence) of RF + UVA, one could apply the FIB + RF + UVA treatment to tissues similar in chemical and molecular composition in other locations in the body. For example, a tendon is connective tissue that heals very slowly due to little vascularization.<sup>56</sup> Because connective tissues like tendons are composed mainly of Coll-I,<sup>57,58</sup> and contain other glycoproteins and proteoglycans, such as Dec,<sup>59,60</sup> the FIB + RF + UVA treatment could be applied to create crosslinks

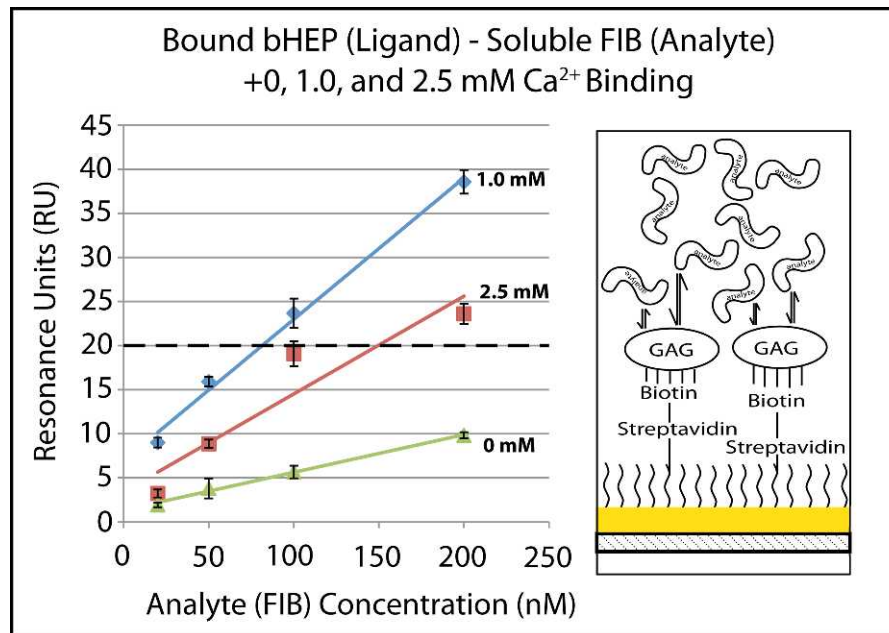


**FIGURE 7.** The relationship between the response of immobilized bHEP and concentration of the analyte (FIB + nil, 1.0, or 2.5 mM  $\text{Ca}^{2+}$ ). No binding occurred between immobilized bHEP and FIB in the absence of  $\text{Ca}^{2+}$  because the response fell below the **bold horizontal dashed line**, which indicates the minimum response necessary for positive binding. The responses of FIB + 1.0 mM and FIB + 2.5 mM  $\text{Ca}^{2+}$  showed a positive linear pattern of response as the concentration of analyte solutions increased.

between the FIB and Coll-I to stabilize the tendon (or other connective tissue) after injury and prevent further damage.

Data collected in our study described two contributing molecular mechanisms of adhesion at play in the FIB + RF + UVA treatment: covalent and noncovalent. First, the SDS-PAGE data demonstrated that FIB forms covalent crosslinks with itself in vitro, in the presence of RF and UVA. This can be concluded from Figure 2a, which shows high molecular weight bands in lanes 8 and 9, when FIB, RF, and UVA all are present simultaneously in solution. In the absence of either RF or UVA (lanes 4–7), FIB shows no change in low molecular weight bands when compared to the control lanes containing only FIB (lanes 2, 3). This suggests that if any FIB + RF solution diffused into the stromal tissue surface during rabbit cornea experimentation and then crosslinked to remaining FIB, either at the glue-tissue interface or within the other stromal surface, the corneal flap could be immobilized. Furthermore, when tested in the presence of Coll-I, the predominant collagen type of the corneal stroma,<sup>16–18</sup> FIB + RF application and UVA irradiation creates covalent crosslinks in vitro. This is evident in Figure 2c because a dramatic difference in band patterns appeared when the only difference was the absence (lane 5) or presence (lane 9) of Coll-I. The dark, very high molecular weight band (arrow in Fig. 2c) corresponds to the  $\gamma$ -chain region of Coll-I (Fig. 2d) and only appears in Figure 2c when Coll-I is present in solution with FIB + RF + UVA. This suggested that when FIB + RF + UVA is applied to a corneal stromal surface, covalent crosslinks occur between and within the glue and stroma, thus further immobilizing the corneal flap.

It is reasonable to ask if the covalent crosslinking detected by in vitro Western blotting between FIB and Coll-I in solution also can be detected in an actual cornea. This is a valid question, as the Coll-I used in vitro is isolated and disorganized, whereas Coll-I, found native in the corneal stroma, is highly organized and bound tightly to proteoglycans, possibly rendering it incapable of bonding with other proteins, such as exogenous FIB. By treating an adult cornea

ex vivo with FIB + RF + UVA and then probing the solubilized cornea with Western blots for appearance of new molecular covalent interactions, these questions of in vitro applicability were addressed. Lanes 1 and 3 of Figure 3 represent samples from de-epithelialized rabbit corneas treated ex vivo with only FIB (no RF or UVA). Lane 1 (probed with FIB-Ab) shows the standard low molecular weight location of FIB chains.<sup>36</sup> Interestingly, lane 3 (probed with Coll-I-Ab) shows a dark low molecular weight band that is dissimilar from the high molecular weight  $\alpha_1/\alpha_2$ ,  $\beta$ , and  $\gamma$  bands observed in Figures 2b and 2d. This may be due to the release and degradation of native collagen by proteases upon the mechanical removal of the epithelium and DM. In a normal adult rabbit cornea, Coll-I mostly is insoluble, even after incubation with acetic acid, but after exposing stromal Coll-I to proteases, it readily becomes soluble.<sup>61,62</sup> Therefore, the low molecular weight band observed in Figure 3, lanes 3 and 4 is likely to represent the most easily extractable soluble degradation product of stromal Coll-I. It should be noted that the soluble protease fragment of Coll-I, released during the 30 minutes of incubation + 30 minutes of irradiation phases of ex vivo cornea treatment, was capable of undergoing extensive crosslinking to form higher molecular weight molecules upon exposure to RF + UVA (Fig. 3, lane 4). Additionally, these ex vivo data duplicated the findings of the in vitro study in that crosslinking was observed only in the extracts of native corneas that had been treated ex vivo with FIB + RF + UVA (Fig. 3, lanes 2, 4). The appearance of similar molecular weight bands in lanes using separate antibodies for FIB and Coll-I suggests that covalent interactions occur between FIB of the tissue glue and Coll-I of the native rabbit corneal stroma (Fig. 3, arrows in lanes 2, 4).

In addition to detecting covalent interactions from SDS-PAGE and WB studies, SPR data suggest that numerous noncovalent interactions contribute to adhesion of stromal surfaces, such as those created by the intrastromal incision during LASIK surgery. Three (Coll-I, Dec, and DS) of the six

molecules that showed binding to soluble FIB are found in stromal tissue, which suggests FIB present in tissue glue not only is interacting covalently with stromal Coll-I in the presence of RF and UVA, but may be interacting first noncovalently with stromal Coll-I, Dec, and DS in the absence of any RF or UVA. These noncovalent interactions are dependent on the presence of  $Zn^{2+}$ , a normal component of the cornea: the dry weight of divalent zinc cation in the human cornea is 41  $\mu\text{g/g}$ ,<sup>63,64</sup> or, when adjusted for the dry weight<sup>65</sup> and volume<sup>66</sup> of a whole human cornea, approximately 0.09 nM, a lower concentration than used here and in earlier studies.<sup>47-49</sup> Furthermore, studies show that metalloenzymes native to the cornea require zinc for regular function,<sup>64,67-69</sup> suggesting that the normal concentration of zinc cation in the cornea is sufficient to mediate chemical processes intra-, and extracellularly.

Results collected in our study are supported by several previous studies about noncovalent macromolecular interactions. For example, it would be expected that DS and CSA would bind to similar molecules, as they have very similar molecular structures.<sup>32,70</sup> However, that is not the case, because polysaccharides with repeating L-iduronic acid residues (DS and HS) have the ability to bind more proteins than do polysaccharides with repeating D-glucuronic acid residues (CSA).<sup>71</sup> These results correspond directly to those collected here: bDS and bHS bound FIB, whereas CSA did not. Also, it has been shown that a protein-protein interaction between Coll-I and cartilage oligomeric matrix protein (COMP) is promoted when the divalent cation  $Zn^{2+}$  (or  $Ni^{2+}$ ) is present, whereas the presence of other divalent cations, such as  $Ca^{2+}$ ,  $Mg^{2+}$ , or  $Mn^{2+}$ , does not facilitate this binding.<sup>47</sup> Again, in our study, similar results were observed. FIB bound Coll-I in the presence of  $Zn^{2+}$ , but not in the presence of two concentrations of  $Ca^{2+}$ . Future studies could determine the optimal concentration of  $Zn^{2+}$  for each of the proteins and GAGs in Table 2 in their interactions with FIB.

In conclusion, data in our study suggested that adhesion observed in rabbit corneas is caused partly by covalent bonds between FIB and Coll-I in the presence of RF and UVA light, and partly by noncovalent interactions between FIB and stromal molecules, such as Coll-I, Dec, and DS, especially in the presence of  $Zn^{2+}$ , even in the absence of RF and UVA. These data represented a starting point in the search for definitive mechanisms explaining the adhesive effects caused by the FIB + RF + UVA treatment and in no way are meant to be a comprehensive look at all possible underlying mechanisms. It is possible that the noncovalent interactions detected here may precede and facilitate subsequent formation of covalent crosslinks formed in the presence of RF + UVA, that is a synergistic relationship,<sup>72</sup> especially since there are  $Zn^{2+}$ -dependent enzymes<sup>73</sup> active in the corneal stroma that have been shown to function at a  $Zn^{2+}$  concentration (0.1 nM<sup>74</sup>) similar to that which we have calculated above (0.09 nM) exists in the corneal stroma. However, that must be elucidated by subsequent studies.

## References

- Littlechild S, Brummer G, Zhang Y, Conrad GW. Fibrinogen, riboflavin and UVA to immobilize a corneal flap - conditions for tissue adhesion. *Invest Ophthalmol Vis Sci.* 2012;53:4011-4020.
- Spoerl E, Huhle M, Seiler T. Induction of cross-links in corneal tissue. *Exp Eye Res.* 1998;66:97-103.
- Hill T, Redmond RW, Kockevar IC. Photosensitized cross-linking of collagen: mechanistic approaches to improved tissue welding. In: *Papers from the First Internet Conference on Photochemistry and Photobiology*. Lawrence, KS: American Soc. for Photobiology; 1998.
- Kato Y, Uchida K, Kawakishi S. Aggregation of collagen exposed to UVA in the presence of riboflavin: plausible role of tyrosine modification. *Photochem Photobiol.* 1994;59:343-349.
- Zhang Y, Conrad A, Conrad GW. Effects of ultraviolet-A and riboflavin on the interaction of collagen and proteoglycans during corneal cross-linking. *J Biol Chem.* 2011;286:13011-13022.
- Khadem J, Truong T, Ernest JT. Photodynamic biologic tissue glue. *Cornea.* 1994;13:406-410.
- Kamaev P, Friedman MD, Sherr E, Muller D. Photochemical kinetics of corneal cross-linking with riboflavin. *Invest Ophthalmol Vis Sci.* 2012;53:2360-2367.
- McCall AS, Kraft S, Edelhofer HF, et al. Mechanisms of corneal tissue cross-linking in response to treatment with topical riboflavin and long-wavelength ultraviolet radiation (UVA). *Invest Ophthalmol Vis Sci.* 2010;51:129-138.
- Brummer G, Littlechild S, McCall S, Zhang Y, Conrad GW. The role of nonenzymatic glycation and carbonyls in collagen cross-linking for the treatment of keratoconus. *Invest Ophthalmol Vis Sci.* 2011;52:6363-6369.
- Timpl R, Rohde H, Robey PG, Rennard SI, Foidart JM, Martin GR. Laminin-a glycoprotein from basement membranes. *J Biol Chem.* 1979;254:9933-9937.
- Timpl R, Glanville RW, Wick G, Martin GR. Immunohistochemical study on basement membrane (type IV) collagens. *Immunology.* 1979;38:109-116.
- Hassell JR, Robey PG, Barrach HJ, Wilczek J, Rennard SI, Martin GR. Isolation of a heparan sulfate-containing proteoglycan from basement membrane. *Proc Natl Acad Sci U S A.* 1980;77:4494-4498.
- Laurie GW, Leblond CP, Martin GR. Localization of type IV collagen, laminin, heparan sulfate proteoglycan, and fibronectin to the basal lamina of basement membranes. *J Cell Biol.* 1982;95:340-344.
- Laurie GW, Leblond CP, Martin GR. Light microscopic immunolocalization of type IV collagen, laminin, heparan sulfate proteoglycan, and fibronectin in the basement membranes of a variety of rat organs. *Am J Anat.* 1983;167:71-82.
- Grant DS, Leblond CP. Immunogold quantitation of laminin, type IV collagen, and heparan sulfate proteoglycan in a variety of basement membranes. *J Histochem Cytochem.* 1988;36:271-283.
- Newsome DA, Gross J, Hassell JR. Human corneal stroma contains three distinct collagens. *Invest Ophthalmol Vis Sci.* 1982;22:376-381.
- Lee RE, Davison PF. Collagen composition and turnover in ocular tissues of the rabbit. *Exp Eye Res.* 1981;32:737-745.
- Conrad GW, Kelly PT, von der Mark K, Edelhofer HF. A comparative study of elasmobranch corneal and scleral collagens. *Exp Eye Res.* 1981;32:659-672.
- Kjellén L, Lindahl U. Proteoglycans: structures and interactions. *Annu Rev Biochem.* 1991;60:443-475.
- Michelacci YM. Collagens and proteoglycans of the corneal extracellular matrix. *Braz J Med Biol Res.* 2003;36:1037-1046.
- Dunlevy JR, Beales MP, Berryhill BL, Cornuet PK, Hassell JR. Expression of the keratan sulfate proteoglycans lumican, keratocan and osteoglycin/mimecan during chick corneal development. *Exp Eye Res.* 2000;70:349-362.
- Goins KM, Khadem J, Majmudar PA. Relative strength of photodynamic biologic tissue glue in penetrating keratoplasty in cadaver eyes. *J Cataract Refract Surg.* 1998;24:1566-1570.
- Johnsson B, Löfås S, Lindquist G. Immobilization of proteins to a carboxymethyl-dextran-modified gold surface for biospecific

- interaction analysis in surface plasmon resonance sensors. *Anal Biochem.* 1991;198:268-277.
24. Löfås S, Johnsson B. A novel hydrogel matrix on gold surfaces in surface plasmon resonance sensors for fast and efficient covalent immobilization of ligands. *J Chem Soc Chem Commun.* 1990;20:1526-1528.
  25. Stenberg E, Persson B, Roos H, Urbaniczky C. Quantitative determination of surface concentration of protein with surface plasmon resonance using radiolabeled proteins. *J Colloid Interface Sci.* 1991;143:513-526.
  26. Conrad AH, Zhang Y, Tasheva ES, Conrad GW. Proteomic analysis of potential keratan sulfate, chondroitin sulfate A, and hyaluronic acid molecular interactions. *Invest Ophthalmol Vis Sci.* 2010;51:4500-4515.
  27. Sheehan JP, Kobbervig CE, Kirkpatrick HM. Heparin inhibits the intrinsic tenase complex by interacting with an exosite on factor IXa. *Biochemistry.* 2003;42:11316-11325.
  28. Osmond RI, Kett WC, Skett SE, Coombe DR. Protein-heparin interactions measured by BIAcore 2000 are affected by the method of heparin immobilization. *Anal Biochem.* 2002;310:199-207.
  29. Saito A, Munakata H. Detection of chondroitin sulfate-binding proteins on the membrane. *Electrophoresis.* 2004;25:2452-2460.
  30. Lerner L, Torchia DA. A multinuclear NMR study of the interactions of cations with proteoglycans, heparin, and Ficoll. *J Biol Chem.* 1986;261:12706-12714.
  31. Telser A, Robinson HC, Dorfman A. The biosynthesis of chondroitin-sulfate protein complex. *Proc Natl Acad Sci U S A.* 1965;54:912-919.
  32. Conrad HE. Structure of heparan sulfate and dermatan sulfate. *Ann N Y Acad Sci.* 1989;556:18-28.
  33. Hagner-McWhirter A, Lindahl U, Li J. Biosynthesis of heparin/heparan sulphate: mechanism of epimerization of glucuronyl C-5. *Biochem J.* 2000;347:69-75.
  34. Höök M, Lindahl U, Iverius PH. Distribution of sulphate and iduronic acid residues in heparin and heparan sulphate. *Biochem J.* 1974;137:33-43.
  35. Lindahl U, Bäckström G, Malmström A, Fransson LA. Biosynthesis of L-iduronic acid in heparin: epimerization of D-glucuronic acid on the polymer level. *Biochem Biophys Res Commun.* 1972;46:985-991.
  36. McKee PA, Mattock P, Hill RL. Subunit structure of human fibrinogen, soluble fibrin, and cross-linked insoluble fibrin. *Proc Natl Acad Sci U S A.* 1970;66:738-744.
  37. Schuck P. Use of surface plasmon resonance to probe the equilibrium and dynamic aspects of interactions between biological macromolecules. *Annu Rev Biophys Biomol Struct.* 1997;26:541-566.
  38. Fisher RJ, Fivash M. Surface plasmon resonance based methods for measuring the kinetics and binding affinities of biomolecular interactions. *Curr Opin Biotechnol.* 1994;5:389-395.
  39. Sakamoto N, Shioya T, Serizawa T, Akashi M. Direct observation of fibrinogen-heparinoid complexes formation using surface plasmon resonance. *Bioconjug Chem.* 1999;10:538-543.
  40. Marx G, Mou X, Hotovely-Salomon A, et al. Heat denaturation of fibrinogen to develop a biomedical matrix. *J Biomed Mater Res B Appl Biomater.* 2008;84:49-57.
  41. Mihalyi E. Review of some unusual effects of calcium binding to fibrinogen. *Biophys Chem.* 2004;112:131-140.
  42. Moore EW. Ionized calcium in normal serum, ultrafiltrates, and whole blood determined by ion-exchange electrodes. *J Clin Invest.* 1970;49:318-334.
  43. Bushinsky DA, Monk RD. Electrolyte quintet: calcium. *Lancet.* 1998;352:306-311.
  44. Mohri H, Ohkubo T. Fibrinogen binds to heparin: the relationship of the binding of other adhesive proteins to heparin. *Arch Biochem Biophys.* 1993;303:27-31.
  45. Mohri H, Iwamatsu A, Ohkubo T. Heparin binding sites are located in a 40-kd gamma-chain and a 36-kd beta-chain fragment isolated from human fibrinogen. *J Thromb Thrombolysis.* 1994;1:49-54.
  46. Yakovlev S, Gorlatov S, Ingham K, Medved L. Interaction of fibrin(ogen) with heparin: further characterization and localization of the heparin-binding site. *Biochemistry.* 2003;42:7709-7716.
  47. Rosenberg K, Olsson H, Mörgelin M, Heinegård D. Cartilage oligomeric matrix protein shows high affinity zinc-dependent interaction with triple helical collagen. *J Biol Chem.* 1998;273:20397-20403.
  48. Dugan TA, Yang VW, McQuillan DJ, Höök M. Decorin binds fibrinogen in a Zn<sup>2+</sup>-dependent interaction. *J Biol Chem.* 2003;278:13655-13662.
  49. Vu TT, Stafford AR, Leslie BA, Kim PY, Fredenburgh JC, Weitz JI. Histidine-rich glycoprotein binds fibrin(ogen) with high affinity and competes with thrombin for binding to the gamma'-chain. *J Biol Chem.* 2011;286:30314-30323.
  50. Munakata H, Takagaki K, Majima M, Endo M. Interaction between collagens and glycosaminoglycans investigated using a surface plasmon resonance biosensor. *Glycobiology.* 1999;9:1023-1027.
  51. Khadem J, Martino M, Anatelli F, Dana MR, Hamblin MR. Healing of perforating rat corneal incisions closed with photodynamic laser-activated tissue glue. *Lasers Surg Med.* 2004;35:304-311.
  52. Khadem J, Veloso AA Jr, Tolentino F, Hasan T, Hamblin MR. Photodynamic tissue adhesion with chlorin(e6) protein conjugates. *Invest Ophthalmol Vis Sci.* 1999;40:3132-3137.
  53. Goins KM, Khadem J, Majmudar PA, Ernest JT. Photodynamic biologic tissue glue to enhance corneal wound healing after radial keratotomy. *J Cataract Refract Surg.* 1997;23:1331-1338.
  54. Khadem JJ, Dana MR. Photodynamic biologic tissue glue in perforating rabbit corneal wounds. *J Clin Laser Med Surg.* 2000;18:125-129.
  55. Mi S, Dooley EP, Albon J, Boulton ME, Meek KM, Kamma-Lorger CS. Adhesion of laser in situ keratomileusis-like flaps in the cornea: effects of crosslinking, stromal fibroblasts, and cytokine treatment. *J Cataract Refract Surg.* 2011;37:166-172.
  56. Butler DL, Juncosa N, Dressler MR. Functional efficacy of tendon repair processes. *Annu Rev Biomed Eng.* 2004;6:303-329.
  57. Amiel D, Frank C, Harwood F, Fronck J, Akeson W. Tendons and ligaments: a morphological and biochemical comparison. *J Orthop Res.* 1984;1:257-265.
  58. Kannus P. Structure of the tendon connective tissue. *Scand J Med Sci Sports.* 2000;10:312-320.
  59. Frank C, Shrive N, Hiraoka H, Nakamura N, Kaneda Y, Hart D. Optimisation of the biology of soft tissue repair. *J Sci Med Sport.* 1999;2:190-210.
  60. Derwin KA, Soslowsky LJ, Kimura JH, Plaas AH. Proteoglycans and glycosaminoglycan fine structure in the mouse tail tendon fascicle. *J Orthop Res.* 2001;19:269-277.
  61. Freeman IL. Collagen polymorphism in mature rabbit cornea. *Invest Ophthalmol Vis Sci.* 1978;17:171-177.
  62. Welsh C, Gay S, Rhodes RK, Pfister R, Miller EJ. Collagen heterogeneity in normal rabbit cornea. I. Isolation and biochemical characterization of the genetically-distinct collagens. *Biochim Biophys Acta.* 1980;625:78-88.
  63. Grahn BH, Paterson PG, Gottschall-Pass KT, Zhang Z. Zinc and the eye. *J Am Coll Nutr.* 2001;20:106-118.

64. Karcioğlu ZA. Zinc in the eye. *Surv Ophthalmol*. 1982;27:114-122.
65. Hasany SM, Basu PK. Changes of MK medium during storage of human cornea. *Br J Ophthalmol*. 1987;71:477-483.
66. Hedbys BO, Mishima S. The thickness-hydration relationship of the cornea. *Exp Eye Res*. 1966;5:221-228.
67. Berman MB, Manabe R. Corneal collagenases: evidence for zinc metalloenzymes. *Ann Ophthalmol*. 1973;5:1193-1195.
68. Balasubramanian SA, Pye DC, Willcox MD. Are proteinases the reason for keratoconus? *Curr Eye Res*. 2010;35:185-191.
69. Nagase H, Woessner JF Jr. Matrix metalloproteinases. *J Biol Chem*. 1999;274:21491-21494.
70. Saito A, Munakata H. Analysis of plasma proteins that bind to glycosaminoglycans. *Biochim Biophys Acta*. 2007;1770:241-246.
71. Lindahl U, Höök M. Glycosaminoglycans and their binding to biological macromolecules. *Annu Rev Biochem*. 1978;47:385-417.
72. Mulroy L, Kim J, Wu I, et al. Photochemical keratodesmos for repair of lamellar corneal incisions. *Invest Ophthalmol Vis Sci*. 2000;41:3335-3340.
73. Agrawal A, Romero-Perez D, Jacobsen JA, Villarreal FJ, Cohen SM. Zinc-binding groups modulate selective inhibition of MMPs. *ChemMedChem*. 2008;3:812-820.
74. Brejchova K, Liskova P, Hrdlickova E, Filipec M, Jirsova K. Matrix metalloproteinases in recurrent corneal melting associated with primary Sjögren's syndrome. *Mol Vis*. 2009;15:2364-2372.